






Cite this: *J. Mater. Chem. B*, 2017,  
5, 5668

## A mussel-inspired poly( $\gamma$ -glutamic acid) tissue adhesive with high wet strength for wound closure

Wei Chen,<sup>a</sup> Rui Wang,<sup>a</sup>  Tingting Xu,<sup>a</sup> Xuebin Ma,<sup>a</sup>  Zhong Yao,<sup>a</sup> Bo Chi <sup>\*a</sup> and Hong Xu<sup>\*a</sup>

Injectable hydrogels are promising candidates for adhesives because of their ease of administration, minimal invasion, and biocompatibility. While developing surgical adhesives with strong wet tissue adhesion, controlled degradability and mechanical properties, and excellent biocompatibility have still been a significant challenge. Herein, inspired from nature, we report a novel mussel-inspired tissue-adhesive hydrogel composed of poly( $\gamma$ -glutamic acid) and dopamine ( $\gamma$ -PGA-DA) that can bond tissues well and stop bleeding in a wet environment by improving its tissue adhesiveness via a horseradish peroxidase-mediated reaction. The hydrogel exhibited 10–12 fold stronger wet tissue adhesion strength (58.2 kPa) over the clinically used fibrin glue and more effective hemostatic ability following liver impalement in animal models (41.2% reduction in the average amount of bleeding compared with fibrin glue). In addition, the hydrogels demonstrated controlled gelation time, swelling ratio, microscopic morphology, biodegradability and tissue-like elastomeric mechanical properties, and exhibited excellent cyto/tissue-compatibility. The overall results suggest that the  $\gamma$ -PGA-DA hydrogels can be considerably applied as promising wet-resistant adhesives and hemostatic materials.

Received 24th March 2017,  
Accepted 14th June 2017

DOI: 10.1039/c7tb00813a

rsc.li/materials-b

## Introduction

Wound closure and healing after traumatic or surgical injury is of significant clinical and research importance. An appropriate tissue connector must hold the edges of injured tissues close together to support healing and also stop bleeding when resisting against tensile forces.<sup>1–3</sup> Even though common mechanical methods and conventional products are convenient for wound closure, their application has some limitations and drawbacks such as being painful for patients and hard to integrate well with the irregularly shaped defects. In addition, secondary injury caused by replacing the dressing, poor biocompatibility, and biodegradability severely impedes the application of these products for wound closure.<sup>4–6</sup> Injectable hydrogel tissue adhesives are promising candidates for wound management because of their suitability for irregular wounds, good biocompatibility, and minimally invasive injection procedures.<sup>7–10</sup> No biocompatible and biodegradable products that strongly bond to tissues and function well under wet and highly dynamic physiological

environments have been clinically approved, despite the progress in and demand for hydrogel-based hemostatic materials.<sup>11–13</sup>

Mussel-inspired hydrogel tissue adhesives have received considerable interest because of their robust adhesion and cohesive strength in a wet environment.<sup>14–16</sup> Various synthetic-material-based tissue adhesives (acrylates and poly(ethylene glycol) (PEG) hydrogels) and biological adhesives (fibrin glues, polysaccharides, and proteins) have been extensively developed.<sup>13,17</sup> Hydrogels derived from natural polymers would be more acceptable due to their good biocompatibility and biodegradability.<sup>13,18</sup> Chitosan is currently the most frequently investigated natural polymer for hemostatic material because of its inherent hemostasis ability.<sup>8,19,20</sup> Lee *et al.* developed several mussel-inspired chitosan-based hemostatic materials to support hemostasis and wound healing.<sup>1,7</sup> However, the poor water solubility, potential antigenicity, and immunogenicity of chitosan limits its application, because these properties are not suitable for internal use.<sup>8,19,21</sup>

Poly( $\gamma$ -glutamic acid) ( $\gamma$ -PGA) is a natural homo-polyamide linked by a peptide bond between the  $\alpha$ -amino and  $\gamma$ -carboxyl groups.<sup>22,23</sup> It has been manufactured commercially through fermentation by a *Bacillus subtilis* strain in our laboratory and applied in various fields, such as agriculture, cosmetic, and medical materials.<sup>23–25</sup>  $\gamma$ -PGA possesses many excellent properties, such as good water solubility, biocompatibility, biodegradability, and high molecular weight ( $\approx 1$  million Da) compared with the

<sup>a</sup> State Key Laboratory of Materials-Oriented Chemical Engineering, Nanjing Tech University, No. 30 South Puzi Road, Pukou District, Nanjing 211816, China.  
E-mail: chibo@njtech.edu.cn, xuh@njtech.edu.cn

<sup>b</sup> School of Chemical Engineering, Nanjing University of Science and Technology, Nanjing 210094, China

molecular weights of other synthetic or natural polymers, such as PEG, hyaluronic acid, dextran, and alginate, which range from 10 kDa to 100 kDa.<sup>22,26</sup> The numerous carboxyl groups in the side-chain facilitate the functionalization of  $\gamma$ -PGA using various crosslinking moieties to fabricate scaffolds that can mimic the three-dimensional network of the extracellular matrix.<sup>27–29</sup>

Moreover,  $\gamma$ -PGA has strong hydrophilicity, edibility, and nontoxicity, which can promote cell adhesion, binding, and proliferation.<sup>28,29</sup> Thus,  $\gamma$ -PGA, combined with catechol, is an ideal candidate for designing mussel-inspired adhesives in a wet environment.

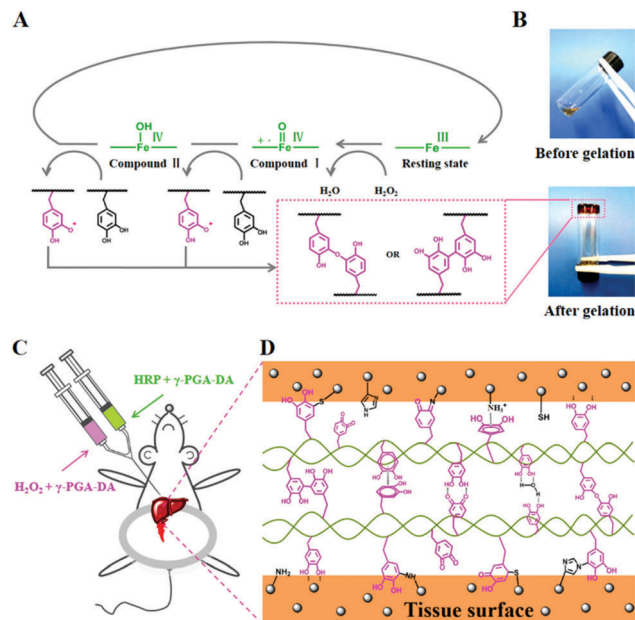
The majority of in-depth studies on catecholic crosslinking have primarily focused on catechol- $\text{Fe}^{3+}$  coordination or chemically induced oxidation to form reactive quinones using  $\text{NaIO}_4$ .<sup>10,30–32</sup> However, the instability of metal-catechol coordination of the structure and potential cytotoxicity of  $\text{NaIO}_4$  has limited further applications of these materials.<sup>13,18</sup> Hydrogels formed *in situ* via the enzymatic crosslinking method has received much attention as an injectable medical device because of the tuning of the gelation rate and the mechanical strength and good biocompatibility of the resulting gels.<sup>33,34</sup> In particular, horseradish peroxidase (HRP) is an efficient and specific biocatalyst ubiquitously derived from horseradish roots. This catalyst has been extensively utilized to fabricate phenol-functionalized polymer hydrogel systems.<sup>33–35</sup> However, among several mussel-inspired *in situ* gelling systems, HRP-catalyzed crosslinked tissue adhesive hydrogels are rarely reported.<sup>16</sup>

In this study, inspired by mussel, we reported a facile strategy by HRP crosslinking for the *in situ* formation of hydrogels based on  $\gamma$ -PGA conjugated with dopamine (DA) as a biomimetic bioadhesive for local hemostasis application (Scheme 1A). DA is an analog of 3,4-dihydroxyphenyl-L-alanine (DOPA), which plays a critical role in the wet adhesion of mussel. DA was selected as the functional group, because it could not only increase the tissue cohesive force but also enhance the binding of blood platelet.<sup>14,36,37</sup> We systematically investigated the influence of the polymer, HRP,  $\text{H}_2\text{O}_2$  content, and the degree of substitution (DS) of DA on the gelation time, microscopic morphology, mechanical properties, and biodegradation rate. In addition, the multiple interfacial interactions, including hydrogen bonding,  $\pi$ - $\pi$ , and/or cation- $\pi$  interaction, and covalent interaction, between the hydrogels and tissue endowed the  $\gamma$ -PGA-DA hydrogels with excellent tissue-adhesion performance even in a highly wet environment (Scheme 1D). Importantly, the hemorrhaging liver mouse models demonstrated that the hydrogels could rapidly seal a hemorrhaging wound and prevent bleeding. Meanwhile, the hydrogel effectively supported the adhesion, proliferation, and migration of epidermal cells, suggesting good biocompatibility. Consequently, the  $\gamma$ -PGA-DA hydrogels showed significant potential for hemostatic materials, tissue adhesives, and other biomedical applications.

## Experimental

### Materials

Poly( $\gamma$ -glutamic acid) ( $\gamma$ -PGA,  $M_w = 700$  kDa) was obtained from Shineking Biotechnology Co., Ltd (Nanjing, China). Dopamine



**Scheme 1** (A) Possible mechanism of the enzymatic crosslinking of  $\gamma$ -PGA-DA conjugates. (B) Gross view of the  $\gamma$ -PGA-DA hydrogel before (top) and after (bottom) gelation. (C) Schematic of the *in vivo* hemostatic ability test. (D) Schematic illustration of potential mechanisms of  $\gamma$ -PGA-DA hydrogel tissue adhesion.

hydrochloride (DA), hydrogen peroxide ( $\text{H}_2\text{O}_2$ , 30 wt%), horseradish peroxidase (HRP), 1-ethyl-3-(3-dimethylaminopropyl)-carbodiimide hydrochloride (EDC), *N*-hydroxysuccinimide (NHS), and papain ( $6000 \text{ U mg}^{-1}$ ) were all purchased from Aladdin. Fibrin glue was purchased from Hangzhou Pull Biotech Co. Ltd (Hangzhou, China). All the chemicals were of analytical grade and were used without further purification.

### Synthesis of dopamine-modified poly( $\gamma$ -glutamic acid) ( $\gamma$ -PGA-DA)

$\gamma$ -PGA-DA conjugates were synthesized by the modification of  $\gamma$ -PGA with DA under the catalysis of EDC/NHS (Fig. 1A). Briefly,  $\gamma$ -PGA (1.0g, 7.8 mmol in terms of repeating units) was dissolved in 100 mL of distilled water to obtain a 1.0 wt% solution. EDC and NHS were then added to the  $\gamma$ -PGA solution at an equal molar ratio to  $\gamma$ -PGA and stirred for 30 min at pH 5.0, after which a predetermined amount of DA was added. The reaction mixture was purged with nitrogen and stirred for 12 h at room temperature in the dark. As the reaction proceeded, the pH of the mixture was maintained at 5.0 with 1 M NaOH and 1 M HCl. After being dialyzed against distilled water for 3 days in the dark ( $M_w$  cut-off 3500 Da), the final products were lyophilized and stored at  $4^\circ\text{C}$  until use.

### Characterization of $\gamma$ -PGA-DA

$^1\text{H}$  NMR and UV-vis were employed to characterize the degree of substitution (DS) of the products. Firstly,  $\gamma$ -PGA-DA with different substitutions were dissolved in deuterated water and characterized using  $^1\text{H}$  NMR (Bruker Avance 400 MHz) spectra. The degree of substitution (DS) was defined as the number of

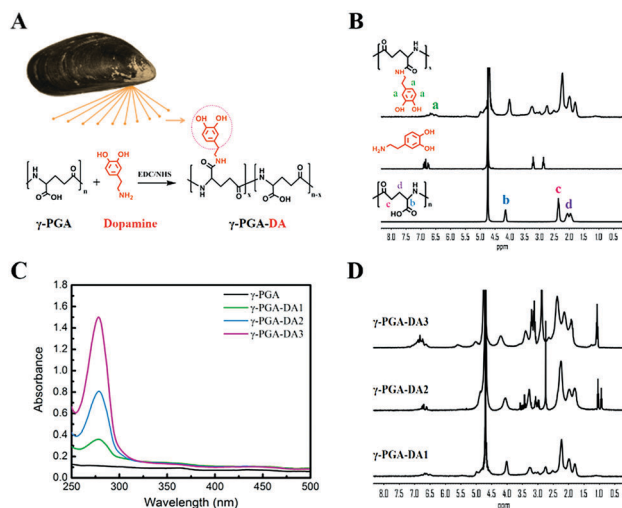


Fig. 1 (A) Synthesis of  $\gamma$ -PGA-DA conjugates by coupling  $\gamma$ -PGA with dopamine. (B)  $^1\text{H}$  NMR (400 MHz,  $\text{D}_2\text{O}$ ) spectra of  $\gamma$ -PGA, DA and  $\gamma$ -PGA-DA. (C) UV-vis (250–500 nm) spectra of  $\gamma$ -PGA,  $\gamma$ -PGA-DA1,  $\gamma$ -PGA-DA2 and  $\gamma$ -PGA-DA3. (D)  $^1\text{H}$  NMR (400 MHz,  $\text{D}_2\text{O}$ ) spectra of  $\gamma$ -PGA-DA1,  $\gamma$ -PGA-DA2 and  $\gamma$ -PGA-DA3.

substituents per 100 carboxyl groups in  $\gamma$ -PGA, and it was determined by comparing the integral areas of signals at  $\delta$  6.5 and 7.2 ppm (catechol) to  $\delta$  3.9–4.3 ppm ( $\gamma$ -PGA  $\alpha$ -protons). Furthermore, the catechol contents of the  $\gamma$ -PGA-DA conjugates were further measured quantitatively at 280 nm using a UV-visible spectrophotometer (Cary 60 UV-Vis, Agilent Technologies). The degree of substitution of the products and their preparation parameters are illustrated in Table 1.

### Enzymatic crosslinking of $\gamma$ -PGA-DA hydrogels and gelation time measurement

As a typical example, the  $\gamma$ -PGA-DA solution was prepared by dissolving  $\gamma$ -PGA-DA in phosphate buffered saline (PBS: 0.01 M, pH 7.4). Predetermined amounts of HRP and  $\text{H}_2\text{O}_2$  solution were added and homogeneously mixed in vials. The final concentration of  $\gamma$ -PGA-DA, HRP and  $\text{H}_2\text{O}_2$  was 8.0 wt%, 20.0  $\text{U mL}^{-1}$ , and 10.0 mM, respectively. The mixture was incubated at 37  $^\circ\text{C}$  and gelled quickly. In order to evaluate the dependence of gel time on the HRP and  $\text{H}_2\text{O}_2$ , each polymer solution (300  $\mu\text{L}$ , 8% (w/v)) in PBS (0.01 M, pH 7.4) was mixed with different concentrations of HRP (1.6–40.0  $\text{U mL}^{-1}$ ) and  $\text{H}_2\text{O}_2$  (2.6–105.0 mM) in 5 mL vials, and then the mixture was incubated at 37  $^\circ\text{C}$  immediately. The gelation time of the  $\gamma$ -PGA-DA hydrogels was determined by the vial tiling method and defined as the time at which no flow was observed.

Table 1 Synthesis of  $\gamma$ -PGA-DA with different degrees of substitution

Samples	Theoretical feeding molar ratio		DS (%)	Phenolic content ( $\mu\text{mol g}^{-1}$ )
	$\gamma$ -PGA:EDC:NHS	DA: $\gamma$ -PGA		
$\gamma$ -PGA-DA1	1:1:1	0.3	10.0	701.8
$\gamma$ -PGA-DA2	1:1:1	0.5	16.1	1068.1
$\gamma$ -PGA-DA3	1:1:1	1.0	35.6	2010.7

### Rheological experiments

Rheological experiments of the hydrogels were performed on a HAAKE Rheometer 600 using a parallel plate (plate diameter = 25 mm, gap = 0.5 mm) in oscillatory mode at 37  $^\circ\text{C}$ . For the kinetic study, 200  $\mu\text{L}$  of the pre-gel solution containing  $\gamma$ -PGA-DA, HRP and  $\text{H}_2\text{O}_2$  was quickly prepared and placed on the plate of the rheometer immediately. Silicon oil was placed around the rim to prevent the evaporation of water. The storage modulus ( $G'$ ) and loss modulus ( $G''$ ) were recorded as a function of time at a frequency of 1 Hz and a strain of 1%. All the experiments were performed within the linear viscoelastic region.

### Morphology of the hydrogels

The morphology of the hydrogels was examined *via* scanning electron microscopy (SEM, S-3400N II). In a typical procedure, hydrogel specimens were immersed in liquid nitrogen, lyophilized, and then cut into thin sections using a sharp blade. The cross-section of the hydrogels was gold-coated and viewed using a microscope.

### Swelling ratio

For the swelling test, the hydrogel samples were prepared by enzymatic crosslinking at 37  $^\circ\text{C}$  for 2 h to ensure complete crosslinking, and the initial weight of the dry hydrogel was measured after being freeze-dried. Subsequently, hydrogels were immersed in 10 mL of PBS solution (0.01 M, pH 7.4) at 37  $^\circ\text{C}$ . After predetermined time intervals, the buffer solutions were removed and the swollen hydrogels were accurately weighed after gently blotting with tissue paper to remove the adhering water. The swelling ratio was calculated using the following equation:

$$\text{Swelling ratio (\%)} = \frac{w_t}{w_0} \times 100\%$$

where  $w_0$  and  $w_t$  are the weights of the initial dry hydrogel and the swollen hydrogel, respectively. The equilibrium swelling ratio was determined until no further weight change was detected. The experiments were performed in triplicate.

### Tissue adhesive strength

Tissue adhesive strength of the hydrogels was investigated using a universal testing machine (M350, Testometric) in accordance with the method modified from ASTM F2255-05.<sup>38</sup> Porcine skins (20 mm in diameter) dehydrated in PBS (0.01 M, pH 7.4) for 1 h were attached to the rubber fixtures with a PBS-soaked gauze to avoid dry conditions. The hydrogels formed with the HRP (40  $\mu\text{L}$ , 20.0  $\text{U mL}^{-1}$ ) and  $\text{H}_2\text{O}_2$  (40  $\mu\text{L}$ , 10.0 mM) solutions were placed on the substrate (bonding area: 20  $\times$  20  $\text{mm}^2$ ), and the additional fixed-skin specimen was immediately stacked up with the prepared hydrogel-skin layer at 37  $^\circ\text{C}$  for 2 h. The adhesive strength was assessed using a universal testing machine equipped with 100 N of load cell at a crosshead speed of 1.3  $\text{mm min}^{-1}$  at room temperature. Each measurement was repeated at least 5 times in order to reduce the experimental error rate. Adhesion strength was calculated in a method of dividing the

maximum load by overlapping contact area. Fibrin glue was also measured under the same conditions as a control adhesive ( $n = 5$ ).

### *In vitro* proteolytic degradation

To test the enzymatic degradation of the hydrogels with different crosslinking ratios, the hydrogels were incubated at 37 °C in PBS (0.01 M, pH 7.4) with and without 0.05 mg mL<sup>-1</sup> of papain after equilibrium for 1 day. At predetermined time intervals, the media were removed and changes in the weight of the hydrogels were recorded. The solution was replaced every day by a fresh solution. The degree of degradation was calculated using the following equation:

$$\text{Weight of hydrogels (\%)} = \frac{w_d}{w_i} \times 100\%$$

where  $w_i$  is the initial weight of the hydrogels and  $w_d$  is the weight of degraded hydrogels.

### *In vitro* cytotoxicity studies

An indirect contact method, according to the ISO10993 standard test, was employed to evaluate the cytotoxicity of  $\gamma$ -PGA-DA hydrogels by using L929 mouse epidermal cells (ECs). Briefly, to each 96-well cell culture plates, 100  $\mu$ L of the pre-gel solution containing different polymer concentrations ([polymer] = 4–8 wt%, [HRP] = 20.0 U mL<sup>-1</sup>, [H<sub>2</sub>O<sub>2</sub>] = 10.0 mM) was added. All the sample solutions were sterilized by filtration *via* 0.22  $\mu$ m syringe filters in advance. After gelling at 37 °C for 4 h, the gels were washed with PBS three times. Subsequently, ECs were seeded at a density of  $1.0 \times 10^5$  cells per well in 200.0  $\mu$ L of medium containing 10 vol% fetal bovine serum (FBS) and 1.0 wt% penicillin–streptomycin and cultured at 37 °C in an incubator with 5% CO<sub>2</sub> for 24 h. Then, on the 1st, 3rd, and 5th day, 50  $\mu$ L of MTT (5.0 mg mL<sup>-1</sup> in PBS) was added to each well of a 96-well plate, and ECs were cultured for another 4 h to allow the formation of formazan crystals. After washing with PBS three times, 150  $\mu$ L of DMSO was added to dissolve the resulting formazan crystals in the dark. The absorbance assay was conducted on a microplate reader at 490 nm. Cells incubated in medium without any hydrogels were used as the control. All measurements were carried out in triplicate. The cell viability was obtained by the formula:

$$\text{Cell viability} = \frac{\text{OD}_{\text{sample}}}{\text{OD}_{\text{control}}} \times 100\%$$

### *In vitro* hemostatic ability test

To evaluate the *in vivo* hemostatic potential of the  $\gamma$ -PGA-DA hydrogels, we used a mouse hemorrhaging liver model.<sup>39,40</sup> In brief, fifteen SD rats (normal SD rat, 180–200 g, 6 weeks, male) were anesthetized by intraperitoneal injection of zoletil and immobilized on a surgical corkboard. As shown in Fig. 8A, the liver of the rat was exposed by abdominal incision and a pre-weighted filter paper was placed beneath the liver. In particular, serous fluid around the liver was carefully removed to prevent inaccuracies in the estimation of the blood weight obtained by the filter paper. Bleeding on the liver was induced using an 18G-needle, and 100  $\mu$ L of the pre-gel solution or fibrin glue

was immediately applied on the surface of the bleeding site. After 2 min, the weight of the filter paper with absorbed blood was measured. No treatment after the liver was pricked with a needle was considered as a negative control. Fibrin glue was used as a hemostatic agent for a positive control. For statistical analysis, we used five SD rats for each experimental group ( $n = 5$ ). All experiments were performed in compliance with the relevant laws and institutional guidelines. Meanwhile, all animal care and experimental studies were reviewed and approved by the Animal Investigation Ethics Committee of Jinling Hospital (Registration number: SYXK2012-0047).

### Statistical analysis

Experimental data were expressed as the mean  $\pm$  standard deviation, with at least three samples. Statistical analyses were performed using one-way ANOVA followed by Tukey's multiple comparison tests, and statistical significance was at  $P < 0.05$ .

## Results and discussion

### Synthesis and characterization of $\gamma$ -PGA-DA

$\gamma$ -PGA-DA conjugates were synthesized by modifying the  $\gamma$ -PGA backbone with dopamine *via* a facile carbodiimide coupling reaction using EDC·HCl and NHS, as shown in Fig. 1A. To protect dopamine from oxidation, the reaction mixture was purged with nitrogen throughout the reaction in the dark. As shown in Fig. 1B, <sup>1</sup>H NMR analysis confirmed the dopamine conjugation to the  $\gamma$ -PGA backbone by showing the appearance of catechol signals at 6.5–7.2 ppm. Compared with  $\gamma$ -PGA, a new absorption peak of UV-vis at 280 nm wavelength is observed in the resultant  $\gamma$ -PGA-DA conjugates, demonstrating the successful incorporation of dopamine. Moreover, no peaks appeared at the wavelength of 395 nm, which indicated that the dihydroxybenzyl (catechol) groups in the  $\gamma$ -PGA-DA conjugates were not oxidized to quinones during the synthesis process (Fig. 1C).<sup>30</sup> To calculate the obtained degree of substitution (DS) of  $\gamma$ -PGA-DA, <sup>1</sup>H NMR and UV-vis were employed to characterize the conjugates. Firstly, the DS was determined by comparing the integral areas of signals at  $\delta$  6.5 and 7.2 ppm (catechol) to  $\delta$  3.9–4.3 ppm ( $\gamma$ -PGA  $\alpha$ -protons) as follows:

$$\text{DS} = \frac{I_{(6.5-7.2)}}{I_{(3.9-4.3)} \times 3} \times 100\%$$

Then, to validate the DS obtained from <sup>1</sup>H NMR, the catechol group contents of the conjugates were measured quantitatively at the absorbance of 280 nm *via* the UV-vis spectrum. The catechol group contents of conjugates were 701.8, 1068.1 and 2010.7  $\mu$ mol g<sup>-1</sup>, respectively, which is consistent with the <sup>1</sup>H NMR results.  $\gamma$ -PGA-DA conjugates with DS<sub>catechol</sub> contents of 10.0, 16.1 and 35.6% were synthesized by varying the feeding molar ratio of DA to  $\gamma$ -PGA (Fig. 1D and Table 1). The theoretical feeding molar ratios of DA/ $\gamma$ -PGA (mol%) were 30, 50 and 100%, and the measured DS values were 10.0, 16.1 and 35.6%, respectively. Changing the molar feeding ratios of the primary amine group in dopamine to the carboxyl group in poly( $\gamma$ -glutamic acid) could adjust the catechol group contents in  $\gamma$ -PGA-DA conjugates.



In particular, upon increasing the DA/ $\gamma$ -PGA feeding ratios, the conversion degree of the conjugation significantly decreased. The results showed that a decrease in the conversion degree of dopamine could be attributed to the steric hindrance of the benzene rings that hindered the reaction between DA and  $\gamma$ -PGA.

### Enzymatic crosslinking and gelation time of $\gamma$ -PGA-DA hydrogels

The formation of the  $\gamma$ -PGA-DA hydrogels *via* enzymatic crosslinking is similar to the enzymatic crosslinking of phenol-modified polymers (Scheme 1A).<sup>35</sup> The HRP-mediated catalytic cycle of catechol is initiated by the interaction between  $\text{H}_2\text{O}_2$  and the resting ferric state of HRP [Fe(III)], which generates compound I. With catechol as a reducing substrate, compound I is a high oxidation-state intermediate with a cation radical and converted to compound II after the first one-electron reduction. Then, compound II returns to its resting state *via* the second one-electron reduction step. The generated catechol radicals enable the formation of intermolecular covalent linkages through either carbon-carbon bonds between *ortho*-carbons of the aromatic ring or through carbon-oxygen bonds between *ortho*-carbons and phenolic oxygen.<sup>35,40</sup> Consequently, the reaction mechanism shows that one equivalent of  $\text{H}_2\text{O}_2$  is consumed to two equivalents of catechol radicals at a fixed HRP concentration in a complete catalytic cycle.

Gelation time plays a key role in the design of injectable scaffolds and fulfilling clinical requirements. This parameter should be short and controllable enough to prevent the superfluous diffusion of gel precursors or needle clogging.<sup>41</sup> However, hydrogel should bind or adhere to the wound tissue under moist conditions and maintain its suitable integrity despite the fast gelation.<sup>42</sup> The gelation time was measured at various concentrations of HRP,  $\text{H}_2\text{O}_2$ , and the polymer to investigate the relationship between the crosslinking rate or degree and the number of generated phenoxyl radicals. Gelation time was determined by the vial tilting method and defined as the time at which no flow was observed (Scheme 1B). Fig. 2A shows the effect of  $\text{H}_2\text{O}_2$  concentration on gelation time of  $\gamma$ -PGA-DA hydrogels. In addition, the polymer concentration remains constant at 8.0 wt% and a DS of 16.1%, while the HRP concentration remains constant at 20.0 U mL<sup>-1</sup>. No stable gel formed when polymer solutions with a final  $\text{H}_2\text{O}_2$  concentration less than 2.6 mM were measured. This phenomenon is due to the low crosslinking density and incomplete network structure. The gelation time decreased gradually from 45 s to 25 s when  $\text{H}_2\text{O}_2$  concentration was increased from 2.6 mM to 10.5 mM. However, a further increase in  $\text{H}_2\text{O}_2$  concentration from 10.5 mM to 105 mM showed that gelation time was not reduced but increased drastically from 25 s to 237 s. This phenomenon was previously observed in the HRP-catalyzed gelling of phenol-modified polymers, which should be attributed to the possible loss in catalytic activity of HRP due to an excess in  $\text{H}_2\text{O}_2$ , resulting in slow crosslinking. Fig. 2B shows the effect of HRP concentration on the gelation time of the  $\gamma$ -PGA-DA hydrogels. Furthermore, polymer concentration also remained constant at 8.0 wt% and a DS of 16.1%, while a constant  $\text{H}_2\text{O}_2$  concentration of 10.0 mM was chosen for this study because a faster crosslinking

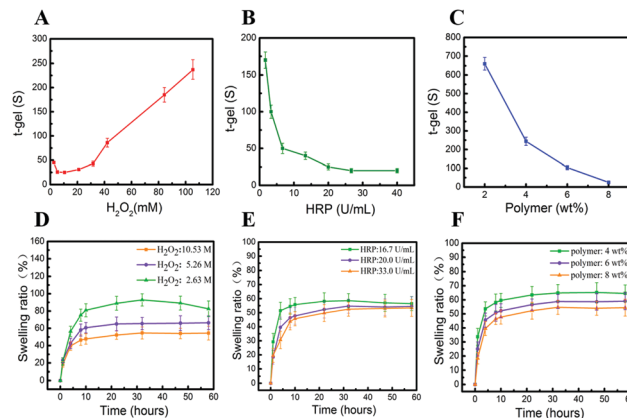


Fig. 2 Gelation time as a function of  $\text{H}_2\text{O}_2$  (A), HRP (B) and polymer concentration (C). Influence of  $\text{H}_2\text{O}_2$  (D), HRP (E) and polymer (F) concentration on the swelling properties of the  $\gamma$ -PGA-DA hydrogel.

rate was obtained at this concentration (Fig. 2A). Gelation time decreased drastically from 170 s to 20 s when HRP concentration was increased from 1.6 U mL<sup>-1</sup> to 40.0 U mL<sup>-1</sup>, which should be ascribed to the fact that higher concentration of HRP accelerated the generation of catechol free radicals, resulting in a faster gelation rate. Fig. 2C shows the effect of polymer concentration on gelation time. The gelation time decreased drastically from 660 s to 25 s as the polymer concentration was increased from 2.0 wt% to 8.0 wt% at a constant  $\text{H}_2\text{O}_2$  concentration of 10.0 mM and a constant HRP concentration of 20.0 U mL<sup>-1</sup>. In this study, the number of reactive groups per unit volume and crosslinking density increased with polymer content, resulting in accelerated gelation and short gelation time. These results suggest that the crosslinking rates of  $\gamma$ -PGA-DA hydrogels could be fairly well controlled by simply changing the concentrations of  $\text{H}_2\text{O}_2$ , HRP, and the polymer.

### Rheological properties of $\gamma$ -PGA-DA hydrogels

The kinetics of the gelation process of  $\gamma$ -PGA-DA was evaluated under physiological conditions (37 °C, pH 7.4) and investigated in a time sweep experiment using a stress-controlled rheometer. We selected the fixed polymer concentration of 6.0 wt% to obtain suitable gelation time for rheological measurements (Fig. 2C). For the kinetic study, 200  $\mu$ L of the pre-gel solution containing  $\gamma$ -PGA-DA (6.0 wt%), HRP (20.0 U mL<sup>-1</sup>), and  $\text{H}_2\text{O}_2$  (10.0 mM) was quickly prepared and immediately placed on the plate of the rheometer. Then, the storage modulus ( $G'$ ) and the loss modulus ( $G''$ ) were recorded as a function of time at a frequency of 1 Hz and a strain of 1%. This test was performed by an amplitude sweep test to determine the linear viscoelastic region of *in situ* crosslinked hydrogels prior to the time sweep test (Fig. 3A). Fig. 3B shows that, at the beginning of the time sweep experiment, the  $G''$  value was higher than the  $G'$  value, indicating a viscous fluid. Both  $G'$  and  $G''$  increased rapidly along with time because of the crosslinking reaction, and these moduli crossover at a reaction time of 60 s for  $G'$  increased faster than  $G''$ . The crossover point is generally considered as the gelation point, which is the transition point from a viscous

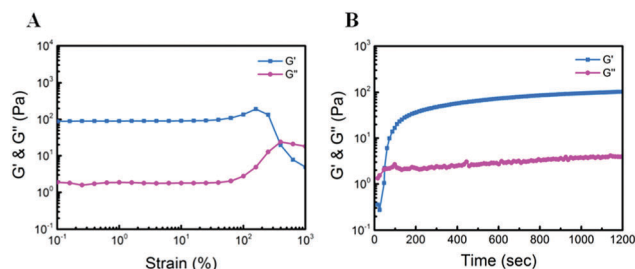


Fig. 3 Rheometric analysis of  $\gamma$ -PGA-DA hydrogels. (A) The strain sweep of the  $\gamma$ -PGA-DA hydrogels. (B) Time dependence of storage modulus ( $G'$ ) and loss modulus ( $G''$ ) of a 6.0 wt%  $\gamma$ -PGA-DA solution (DS = 16.1%) in the presence of HRP (20.0 U mL<sup>-1</sup>) and H<sub>2</sub>O<sub>2</sub> (10.0 mM) at 37 °C. The oscillation frequency was set at 1 Hz.

liquid to a viscoelastic solid.  $G'$  remained larger than  $G''$  with prolonged time, indicating that the elastic component of the system dominates the viscous component. Subsequently, the two moduli of the hydrogels eventually reached a plateau and remained constant at approximately 600 s, suggesting the completion of gelation and the formation of a stable hydrogel. The observed gel is consistent with the vial tilting method (Fig. 2C), because approximately 20 s were required to load the sample before the rheological test.

#### Swelling behavior, inner morphology, and degradation of $\gamma$ -PGA-DA hydrogels

The swelling property of the hydrogels is an important parameter that presents the efficiency of oxygen and nutrient transfer within the scaffold.<sup>43</sup> In addition, many other properties and the applicability of hydrogels are also drastically influenced by the swelling properties.<sup>28</sup> The swelling properties of the  $\gamma$ -PGA-DA hydrogels were also investigated. The hydrogel samples were prepared by enzymatic crosslinking at 37 °C for 2 h to ensure complete crosslinking, and the initial dry hydrogel weight was measured after the hydrogel was freeze-dried. Subsequently, the freeze-dried hydrogels were investigated at predetermined time intervals to obtain the swelling ratio by measuring the changes in wet weight during 60 h of incubation under physiological conditions [in phosphate-buffered saline (PBS) at 37 °C]. Swelling ratios are shown in Fig. 2D–F. All hydrogel samples showed high equilibrium swelling ratio ranging from 52 to 92 under different conditions, suggesting that freeze-dried  $\gamma$ -PGA-DA hydrogels absorbed a large amount of water because of the numerous hydrophilic groups in  $\gamma$ -PGA. Fig. 2D illustrates that the equilibrium swelling ratio decreased drastically when the H<sub>2</sub>O<sub>2</sub> concentration increased from 2.63 mM to 10.53 mM. The swelling ratio of the hydrogels evidently decreased with increasing H<sub>2</sub>O<sub>2</sub> concentration, which should be attributed to the increased crosslinking density and decreased hydrophilic groups in the polymer chains. Fig. 2E shows that the equilibrium swelling ratio decreased from 58.56 to 53.41 with an increase in the HRP concentration from 1.67 U mL<sup>-1</sup> to 33.33 U mL<sup>-1</sup>. Additionally, the equilibrium swelling ratio of the hydrogels decreased as the polymer concentration increased from 4.0 wt% to 8.0 wt% for the gels synthesized at the same concentrations of HRP and H<sub>2</sub>O<sub>2</sub> but different polymer

concentrations (Fig. 2F). The swelling ratio of the hydrogels is generally related to the crosslinking density and hydrophilicity, and increasing the crosslinking density usually results in a decreased swelling ratio. These results suggest that, in our experimental range, an increase in the H<sub>2</sub>O<sub>2</sub>, HRP, and polymer concentrations led to an increase in the crosslinking density and a decrease in hydrophilic groups. These results are consistent with the results from gelation time measurement (Fig. 2A–C).

The porous structures of the hydrogels used as hemostatic sealants play a major role in hemostasis, because they can absorb the exudates of the wounds and help in increasing the concentration of the red blood cells and plates, enhancing the clotting action.<sup>11</sup> Moreover, the presence of a porous structure affects cell adhesion, migration, and proliferation, as well as the diffusion and supply of nutrients and removal of waste products.<sup>44</sup> The inner morphology of lyophilized  $\gamma$ -PGA-DA hydrogels was observed by SEM (Fig. 4). The cross-sectional SEM images showed that the inner pores of the hydrogels were irregularly shaped. The pore size of the hydrogel decreased rapidly from 50–160  $\mu$ m to 30–95  $\mu$ m as the polymer concentration increased from 4.0 wt% to 8.0 wt% (Fig. 4A–C). The inner morphology was markedly influenced by the polymer concentration of the hydrogels, that is, higher polymer concentration resulted in a tighter network structure and the formation of smaller pore size in the hydrogels. Additionally, the internal morphology of the hydrogels was greatly influenced by H<sub>2</sub>O<sub>2</sub> concentration. As shown in Fig. 4E and F, the average pore size of the hydrogel decreased rapidly from 60–165  $\mu$ m to 40–90  $\mu$ m with increased H<sub>2</sub>O<sub>2</sub> concentration from 2.63 mM to 10.53 mM. This result indicates that the decrease in pore size as H<sub>2</sub>O<sub>2</sub> concentration increased could be ascribed to higher crosslinking density. Furthermore, these results are also closely related to the results from the tests on the gelation time and the swelling ratio. In our study, the pore size of the  $\gamma$ -PGA-DA hydrogels could be easily adjusted by simply changing the concentrations of H<sub>2</sub>O<sub>2</sub> or the polymer, which contributed to the migration of encapsulated cells and efficient exchange of nutrients and metabolites.

The biodegradation properties of the hydrogels play an important role in the design of injectable scaffolds for tissue regeneration.<sup>41</sup> Proteolytic degradation was tested *in vitro* to evaluate the degradation profiles of the  $\gamma$ -PGA-DA hydrogels. For this study, hydrogels with different polymer concentrations were prepared and incubated at 37 °C in 0.01 M PBS solution containing 0.05 mg mL<sup>-1</sup> of papain at predetermined time intervals, and the remaining gel was monitored as a function of time. Additionally, the hydrogel sample incubated without papain was considered as a negative control. Fig. 5 presents that the hydrogels incubated in PBS without papain remained stable for 14 days. By contrast, the hydrogel samples incubated in PBS with 0.05 mg mL<sup>-1</sup> of papain were completely degraded within 14 days because of the decomposition of peptide chains *via* proteolytic degradation. Moreover, the degradation rate decreased upon increasing the concentration of the  $\gamma$ -PGA-DA polymer from 4.0 wt% to 8.0 wt%. For instance, the hydrogels with polymer concentrations of 4.0 wt%, 6.0 wt%, and 8.0 wt% incubated at 37 °C in PBS with the same concentration of

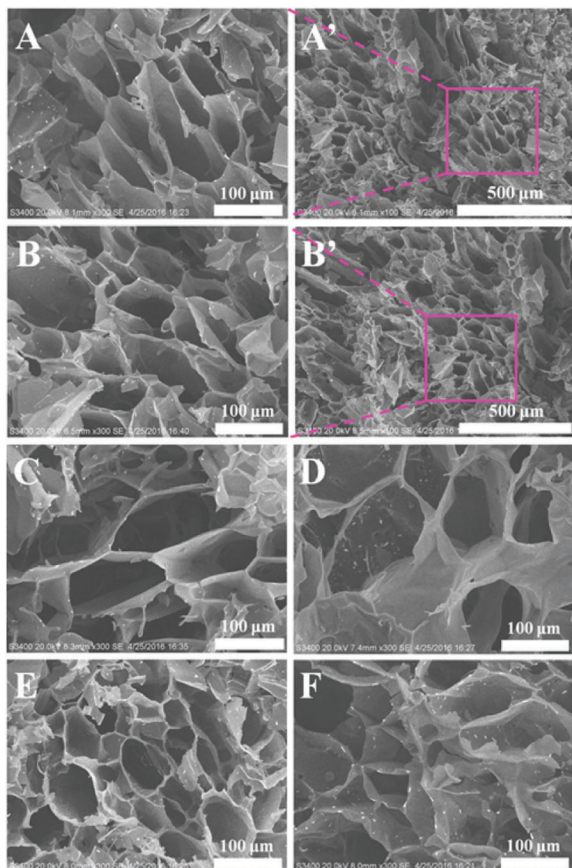


Fig. 4 SEM images of the hydrogels with different polymer contents: 8 wt% (A), 6 wt% (B), and 4 wt% (C). SEM images of the hydrogels with different H<sub>2</sub>O<sub>2</sub> concentrations: 2.63 M (D), 5.26 M (E), and 10.53 M (F).

papain were completely degraded within 7, 10, and 14 days, respectively. This finding may be explained by the fact that, with an increase in polymer concentration, the higher cross-linking density of hydrogels contributed to limit the accessibility of papain to the cleavage sites in the crosslinked hydrogels.

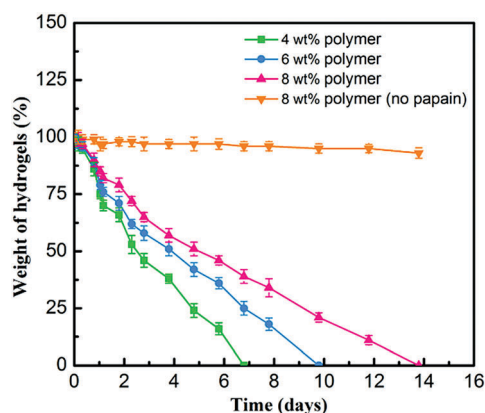


Fig. 5 *In vitro* enzymatic degradation of  $\gamma$ -PGA-DA hydrogels with different polymer contents (4 wt%, 6 wt% and 8 wt%) by papain (300 U mL<sup>-1</sup>) at 37 °C. The hydrogel sample (8 wt%) incubated without papain was considered as a negative control. Remaining wet weights were measured at each time point ( $n = 3$ ).

This feature corresponds to the result of the inner morphology of the hydrogel (Fig. 4).

### Tissue adhesion of $\gamma$ -PGA-DA hydrogels

The adhesion properties of the  $\gamma$ -PGA-DA hydrogels were investigated at different degrees of substitution using the modified ASTM F2255-05 method using a fresh porcine skin tissue surface. This method is a standard technique for testing the strength of tissue adhesives in lap-shear by tension loading.<sup>38</sup> The porcine skin, a common biological organic substrate used in various biomedical experiments to simulate the human dermis, was used as the substrate material, and commercial fibrin glue was used as the control bioadhesive. Samples for the adhesion tests were typically prepared as shown in Fig. 6A. The wet adhesion properties of the  $\gamma$ -PGA-DA hydrogels were evaluated by immersing the porcine skin substrate in PBS solution to keep the skin wet before the adhesion test. The tissues were glued together after pre-gel solution was added on each tissue with overlapping, and then the overlaid porcine skin substrates were compressed by 100 g of weight at 37 °C for 2 h. The relationship between the catechol content and the adhesion strength of  $\gamma$ -PGA-DA hydrogels was examined. The hydrogel samples with different degrees of catechol substitution (10.0%, 16.1%, and 35.6%) were crosslinked in 20.0 U mL<sup>-1</sup> HRP and 10.0 mM H<sub>2</sub>O<sub>2</sub>, and the polymer content was 8.0 wt% for all hydrogel samples. Fig. 7B shows that the average tissue adhesive strength of the control bioadhesive was 5.6 kPa, which was similar to published results.<sup>7,12,19</sup> All hydrogels exhibited greater tissue adhesiveness compared with commercial fibrin glue. Adhesion strength improved drastically from 26.1 kPa to 58.2 kPa when the DS of the hydrogels was increased from 10.0% to 36.5%. This result indicates that the catechol content significantly influenced the adhesion strength of hydrogels. Previous studies showed that a catecholic amino acid is a major component of the mussel foot proteins. This protein is crucial to achieve remarkable underwater adhesion *via* various types of

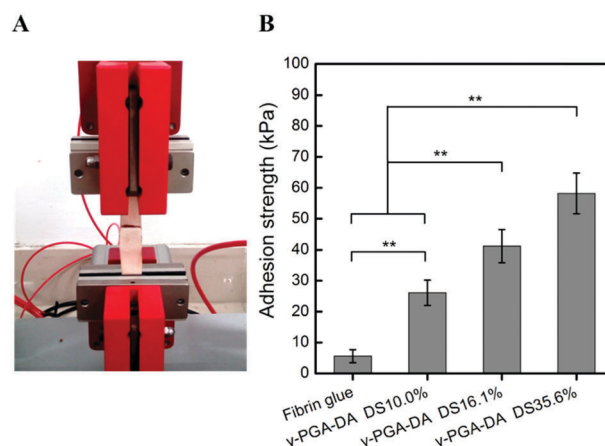


Fig. 6 (A) Tissue adhesion strength of  $\gamma$ -PGA-DA hydrogels. Representative image of a lap shear test using a UTM. (B) Average adhesion strength of  $\gamma$ -PGA-DA hydrogels with different DS values to porcine skin tissue. Fibrin glue as a negative control. ( $n = 5$ , \*\* $p < 0.01$ ).



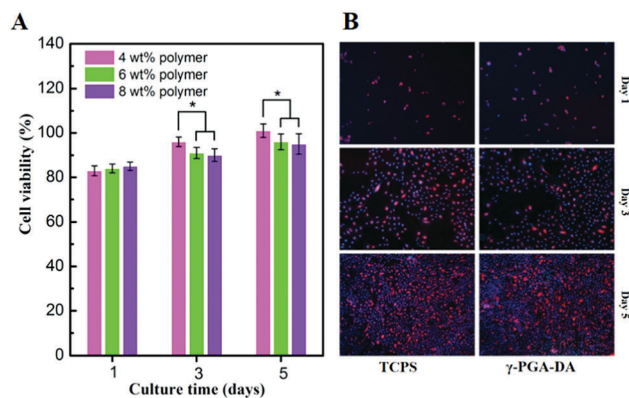


Fig. 7 Cytotoxicity evaluation of  $\gamma$ -PGA-DA hydrogels. (A) Viability of mouse epidermal cells seeded on the surface of  $\gamma$ -PGA-DA hydrogels and cultured for 5 days. (B) Fluorescence image of cells cultured on hydrogels (4 wt% polymer) and TCPS surfaces as a function of culture time. Bare cell culture plate surface (TCPS) as a control. ( $n = 3$ ,  $*p < 0.05$ ).

interactions, including H-bonding, metal–catechol coordination, cation– $\pi$  interaction,  $\pi$ – $\pi$  aromatic interaction and electrostatic interactions.<sup>10,14,16,45</sup> Furthermore, the catechol group is prone to form reactive quinone species through chemically or enzymatically induced oxidation. This species can further undergo Michael addition and Schiff base formation with nucleophiles or radical aryl–aryl coupling with other catechols to achieve peptides and proteins on tissue surface crosslinking (Scheme 1D).<sup>12,16,32,45</sup> These reactions are considered as the potential mechanism of the tissue adhesion of  $\gamma$ -PGA-DA hydrogels. In our study, the adhesion strength of commercial fibrin glue was 5.6 kPa, whereas the maximum adhesion strength of the  $\gamma$ -PGA-DA hydrogels was 58.2 kPa, which is nearly 10 times that of commercial fibrin glue in a wet environment with tissue surfaces. The 58.2 kPa value is higher than those of other previously reported hydrogel adhesives.<sup>7,8,32</sup> Cha *et al.* prepared an adhesive hydrogel using DOPA-containing recombinant mussel adhesive proteins.<sup>31</sup> The results showed that the measured adhesive strength of the  $\text{Fe}^{3+}$ -mediated noncovalent gel was  $\sim 130$  kPa under basic ( $\sim 8.2$ ) pH conditions, and the adhesive strength of the quinone-mediated covalent gel dramatically increased as the curing time before water immersion increased, reaching  $\sim 200$  kPa with 30 min of curing time after treatment with  $\text{NaIO}_4$ . Additionally, many studies have measured the bulk adhesive strength of catechol-incorporated materials. The adhesive strength was found to be from tens of kilopascals to several megapascals, depending on the experimental conditions, such as adherent surface properties or curing environments (temperature, time, and wet/dry).<sup>12,31,46</sup> In this study,  $\gamma$ -PGA-DA hydrogels maintain a balance between gelation time and the strong mechanical and adhesive properties of their strong networks.

### In vitro cytotoxicity studies

The  $\gamma$ -PGA-DA hydrogels were synthesized directly at the bottom of 96-well cell culture plates to investigate the biocompatibility of the hydrogels. L929 mouse epidermal cells were then seeded in the wells, and cell viability was quantitatively determined *via*

MTT assay for 1, 3, and 5 days. Cells incubated in medium without any hydrogels were used as the blank control, and the results were expressed as percentages relative to the data obtained with blank control. The quantitative assessment of the cytotoxicity revealed that all viability values of the cells cultured on the hydrogel surface reached above 80%, suggesting the good cytocompatibility of the  $\gamma$ -PGA-DA hydrogels. As shown in Fig. 7A, there is no statistical difference for cell viability with respect to different polymer concentrations on day 1. Interestingly, it is noteworthy that significant differences were observed on day 3 and 5 ( $P < 0.05$ , with one-way ANOVA test). The cells cultured on the surface of hydrogels (4 wt%) exhibited higher proliferation rates compared with those treated with higher polymer concentration groups (6 wt%, 8 wt%). This phenomenon should be mainly due to the fact that higher porosity with greater pore size ( $60\text{--}165\ \mu\text{m}$ ) contributes to the cell adhesion and proliferation on the gel surface. Additionally, the fluorescence microscopic observation analysis revealed that the cells exhibited normal morphology that could well adhere and proliferate on the surface of hydrogels (4 wt%) (Fig. 7B). It should be noted that higher porosity with greater pore size ( $60\text{--}165\ \mu\text{m}$ ) contributes to the cell adhesion and proliferation on the gel surface.<sup>47–50</sup> This result is related to the results of the swelling behavior and inner morphology measurement, indicating that higher polymer concentration led to tighter network structures and the formation of smaller pore size in the hydrogels. Many studies have demonstrated that designing a suitable pore size of the hydrogel plays a pivotal role in cell survival, proliferation, migration, and differentiation.<sup>48–51</sup> The chemistry of the functional groups, such as abundant carboxyl groups in the side-chain of  $\gamma$ -PGA, also plays an important role in cell adhesion.<sup>28</sup> In this study, we confirmed the excellent biocompatibility of the  $\gamma$ -PGA-DA hydrogels, which should satisfy the requirements of potential materials for biomedical applications.

### In vivo hemostatic ability test

The hemostatic ability of the  $\gamma$ -PGA-DA hydrogels was assessed using a rat liver bleeding model.<sup>39</sup> According to the previously reported method, bleeding was initiated by pricking a liver with an 18-G needle, and we measured the amount of blood released from each group.<sup>7,8,52</sup> In this study, the first group was established as the negative control, because no treatment was applied to this group. The second group, which was treated with commercial fibrin glue, was the positive control, while the third group was applied with  $\gamma$ -PGA-DA hydrogels. Fig. 8A illustrates the photographs of the bleeding sites of each group after 120 s, indicating the excellent hemostatic ability of the hydrogel. The average amount of bleeding within 2 min after the application of the  $\gamma$ -PGA-DA hydrogels was 117.5 mg, whereas those of the fibrin-treated and negative control were 199.7 and 479.7 mg, respectively. These results show that the two groups treated by the hemostatic agents of fibrin glue or  $\gamma$ -PGA-DA hydrogels showed reductions in the bleeding amount (Fig. 8B). A significant difference was found between the hydrogel groups and the control group ( $P < 0.005$ ), which demonstrated that the  $\gamma$ -PGA-DA hydrogels could significantly reduce bleeding efficiently by adhering and covering the



injured site and reduce the average amount of bleeding by 41.2% compared with the control group. Additionally, the difference in the effect of hemostatic agents on liver bleeding with an interval of 30 s to 120 s was monitored continuously and photographs were taken. Fig. 8C shows that both the hemostatic agents of fibrin glue and  $\gamma$ -PGA-DA hydrogels could act as a barrier to blood loss by a fast crosslinking gelled “seal” at the hemorrhaging site. However, in contrast to the control group,  $\gamma$ -PGA-DA hydrogels could capture additional amounts of the spilled bleeding at the site of the wound because of the porous structures. Here, the excellent hemostatic ability of  $\gamma$ -PGA-DA hydrogels is not possible, because, at the hemorrhaging site, the hydrogel could strongly adhere onto the surrounding tissue and instantly form adhesive barriers on the bleeding site. This phenomenon is primarily due to the fact that the remnant catechol quinones could further undergo Michael addition and Schiff base formation with amine, thiol, and imidazole residues in the extracellular matrix proteins and carbohydrates.<sup>16,36,45</sup>

Furthermore, the catechol group can also react with amine- or thiol-functionalized molecules in the blood plasma *via* Schiff-base or Michael addition chemistry, such as serum proteins. This behavior confirms that cells can strongly attach to the hydrogel (Fig. 9).<sup>1,37,53</sup> When the absorbing wound exudates and swells, the local gelled “seal” may also help in localizing the clotting factors from the bloodstream around the wound, thereby enhancing the natural clotting action (Fig. 9).<sup>6,11</sup>

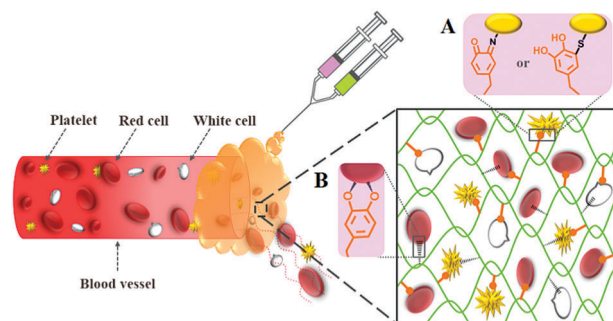


Fig. 9 Schematic representation of a DA-modified poly( $\gamma$ -glutamic acid) hydrogel hemostatic agent. The remnant catechol groups of  $\gamma$ -PGA-DA hydrogels is capable of two types of reaction with functional molecules (e.g., amine or thiol): (A) interfacial covalent crosslinking (e.g., Schiff-base or Michael addition chemistry), and (B) reversible physical crosslinking between DA and functional molecules found in blood plasma.

Moreover, the remnant catechol groups of scaffolds can also enhance the cell adhesion and viability of endothelial cells for vascular tissue engineering.<sup>37,54</sup> These results indicate that  $\gamma$ -PGA-DA hydrogels are beneficial to the promotion of the regeneration of blood vessels at the wound site after the hemostasis procedure. Therefore, we demonstrated that  $\gamma$ -PGA-DA hydrogels show significant potential as local hemostatic agents because of their favorable anti-bleeding effects.

## Conclusions

In summary, we developed novel bio-inspired hydrogels based on  $\gamma$ -PGA to serve as hemostatic materials that can be rapidly formed *in situ* by enzymatic crosslinking. In this work, the DS values and the catechol group contents of  $\gamma$ -PGA-DA conjugates were effectively calculated using  $^1\text{H}$  NMR and UV-vis techniques. Based on the enzymatic crosslinking reaction mechanism, the gelation time, crosslinking density, swelling ratio, microscopic morphology, biodegradation rate, and tissue adhesion properties could be controlled by varying the concentrations of HRP,  $\text{H}_2\text{O}_2$ , and the catechol group contents of  $\gamma$ -PGA-DA conjugates. Importantly, the  $\gamma$ -PGA-DA hydrogel showed good tissue adhesion properties in the wet environment and excellent hemostatic ability *in vivo* compared with fibrin glue. This phenomenon should be ascribed to a fast crosslinking rate and the various types of interactions (e.g., Michael addition, Schiff base, hydrogen bonding, and electrostatic interaction) between the remnant catechol groups of the hydrogel and extracellular matrix proteins or carbohydrates. Furthermore, the hydrogels showed good stability, biodegradation, and biocompatibility *in vitro*. The degradation rates were controlled by adjusting the degree of crosslinking. Thus, these hydrogels can be applied to diverse medical applications, including minimally invasive injectable platforms for tissue adhesives, hemostatic agents, sealants, and drug delivery.

## Acknowledgements

This work was supported by the National Natural Science Foundation of China (31401588, 21476112, 5140030260), the

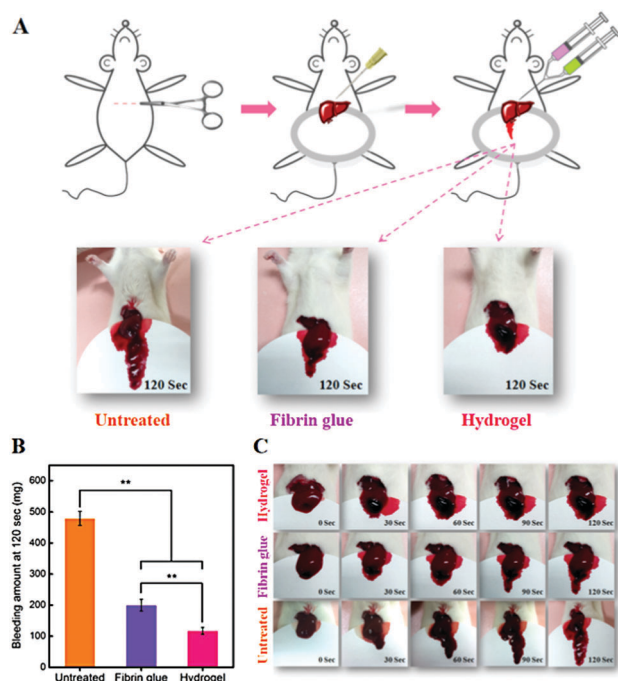


Fig. 8 Hemostatic ability of  $\gamma$ -PGA-DA hydrogels. (A) A schematic illustration of the rat liver hemorrhage model and photographs of the bleeding level of the damaged liver treated by  $\gamma$ -PGA-DA hydrogels or fibrin glue (positive control) and untreated (negative control) at 120 s after the bleeding. (B) The amount of bleeding at 120 s after the injury. (C) Snapshots of a  $\gamma$ -PGA-DA hydrogel or fibrin glue and untreated liver every 30 s for 2 min. ( $n = 3$ ,  $**p < 0.01$ ).

National Basic Research Program of China (973 Program) (2013CB733603), and the State Key Laboratory of Materials-Oriented Chemical Engineering (ZK201606, and ZK201403).

## Notes and references

- M. Shin, S.-G. Park, B.-C. Oh, K. Kim, S. Jo and M. S. Lee, *et al.*, *Nat. Mater.*, 2017, **16**, 147–152.
- A. M. Behrens, M. J. Sikorski and P. Kofinas, *J. Biomed. Mater. Res., Part A*, 2014, **102A**, 4182–4194.
- M. U. Katzenell, B. G. N. Ash, C. A. L. Tapia and M. G. Campino, *Mil. Med.*, 2012, **177**(9), 1065–1068.
- M. J. Larson, M. J. Bowersox, R. C. Lim and J. R. Hess, *Arch. Surg.*, 1995, **130**, 420–422.
- K. King, M. C. Neuffer, E. J. Mcdivitt, D. Rose, K. King, C. C. Cloonan and J. S. Vayer, *Mil. Med.*, 2004, **169**, 716–720.
- M. B. Dowling, R. Kumar, M. A. Keibler, J. R. Hess, G. V. Bochicchio and S. R. Raghavan, *Biomaterials*, 2011, **32**, 3351–3357.
- J. H. Ryu, Y. Lee, H. W. Kong, T. G. Kim, T. G. Park and H. Lee, Catechol-functionalized chitosan/pluronic hydrogels for tissue adhesives and hemostatic materials, *Biomacromolecules*, 2011, **12**, 2653–2659.
- E. Lih, J. S. Lee, K. M. Park and K. D. Park, *Acta Biomater.*, 2012, **8**, 3261–3269.
- N. Lang, M. J. Pereira, Y. Lee, I. Friehs, N. V. Vasilyev, E. N. Feins and k. Ablasser, *Sci. Transl. Med.*, 2014, **6**, 1–8.
- S. Hong, D. Pirovich, A. Kilcoyne, C.-H. Huang, H. Lee and R. Weissleder, *Adv. Mater.*, 2016, **28**, 8675–8680.
- Y. Bu, L. Zhang, J. Liu, L. Zhang, T. Li, H. Shen, X. Wang, F. Yang, P. Tang and D. Wu, *ACS Appl. Mater. Interfaces*, 2016, **8**, 12674–12683.
- M. Mehdizadeh, H. Weng, D. Gyawali, L. Tang and J. Yang, *Biomaterials*, 2012, **33**, 7972–7983.
- N. Annabi, K. Yue, A. Tamayol and A. Khademhosseini, *Eur. J. Pharm. Biopharm.*, 2015, **95**, 27–39.
- H. G. Silverman and F. F. Roberto, *Mar. Biotechnol.*, 2007, **9**, 661–681.
- Y. Liu, K. Ai and L. Lu, *Chem. Rev.*, 2014, **114**, 5057–5115.
- L. Li, W. Smithpong and H. Zeng, *Polym. Chem.*, 2015, **6**, 353–358.
- P. J. M. Bouten, M. Zonjee, J. Bender, S. T. K. Yauw, H. V. Goor, J. C. M. V. Hest and R. Hoogenboom, *Prog. Polym. Sci.*, 2014, **39**, 1375–1405.
- N. Annabi, A. Tamayol, S. R. Shin, A. M. Ghaemaghani, N. A. Peppas and A. Khademhosseini, *Nano Today*, 2014, **9**, 575–589.
- H. S. Whang, W. Kirsch, Y. Zhu, C. Z. Yang and S. M. Hudson, *J. Macromol. Sci. C*, 2005, **45**, 309–323.
- M. B. Dowling, W. Smith, P. Balogh, M. J. Duggan, I. C. Macintire, E. Harris, T. Mesar and S. R. Raghavan, *J. Surg. Res.*, 2015, **193**, 316–323.
- U. A. Sezer, Z. Kocer, B. Aru, G. Y. Demired, M. Gulmez, A. Aktekin, S. Ozkara and S. Sezer, *RSC Adv.*, 2016, **6**, 95189–95198.
- M. Obst and A. Steinbüchel, *Biomacromolecules*, 2004, **5**, 1166–1176.
- I. Bajaj and R. Singhal, *Bioresour. Technol.*, 2011, **102**, 5551–5561.
- B. Tang, H. Xu, Z. Xu, C. Xu, Z. Xu, P. Lei, Y. Qiu, J. Liang and X. Feng, *Bioresour. Technol.*, 2015, **181**, 351–354.
- Z. Xu, P. Lei, X. Feng, S. Li and H. Xu, *J. Agric. Food Chem.*, 2016, **64**, 6257–6266.
- M. Shin, J. H. Ryu, J. P. Park, K. Kim, J. W. Yang and H. Lee, *Adv. Funct. Mater.*, 2015, **25**, 1270–1278.
- M. Matsusaki, T. Serizawa, A. Kishida and M. Akashi, *Biomacromolecules*, 2005, **6**, 400–407.
- M. Matsusaki, H. Yoshida and M. Akashi, *Biomaterials*, 2007, **28**, 2729–2737.
- C. Gentilini, Y. Dong, J. R. May, S. Goldoni, D. E. Clarke, B.-H. Lee, E. T. Pashuck and M. M. Stevens, *Adv. Healthcare Mater.*, 2012, **1**, 308–315.
- N. Holten-Andersen, M. J. Harrington, H. Birkedal, P. L. Bruce, P. B. Messersmith, K. Y. Lee and J. H. Waite, *Proc. Natl. Acad. Sci. U. S. A.*, 2011, **108**, 2651–2655.
- B. J. Kim, D. X. Oh, S. Kim, J. H. Seo, D. S. Hwang, A. Masic, D. K. Han and H. J. Cha, *Biomacromolecules*, 2014, **15**, 1579–1585.
- J. Shin, J. S. Lee, C. Lee, H.-J. Park, K. Yang, Y. Jin, J. H. Ryu, K. S. Hong, S.-H. Moom, H.-M. Chung, H. S. Yang, S. H. Um, J.-W. Oh, D.-I. Kim, H. Lee and S.-W. Cho, *Adv. Funct. Mater.*, 2015, **25**, 3814–3824.
- K. H. Bae and M. Kurisawa, *Biomater. Sci.*, 2016, **4**, 1184–1192.
- Q. V. Nguyen, D. P. Huynh, J. H. Park and D. S. Lee, *Eur. Polym. J.*, 2015, **72**, 602–619.
- J. W. Bae, J. H. Choi, Y. Lee and K. D. Park, *J. Tissue Eng. Regener. Med.*, 2014, **11**, 1225–1232.
- M. Yu, J. Hwang and T. J. Deming, *J. Am. Chem. Soc.*, 1999, **121**, 5825–5826.
- S. H. Ku and C. B. Park, *Biomaterials*, 2010, **31**, 9431–9437.
- S. Kull, M. Eng, I. Martinelli, E. Briganti and P. Losi, *et al.*, *J. Surg. Res.*, 2009, **157**, e15–e21.
- Y. Murakami, M. Yokoyama, H. Nishida, Y. Tomizawa and H. Kurosawa, *Colloids Surf., B*, 2008, **65**, 186–189.
- P. Campomanes, U. Rothlisberger, M. Alfonso-Prieto and C. Rovira, *J. Am. Chem. Soc.*, 2015, **137**, 11170–11178.
- A. Fathi, S. M. Mithieux, H. Wei, W. Chrzanowski, P. Valtchev, A. S. Weiss and F. Dehghani, *Biomaterials*, 2014, **35**, 5425–5435.
- C. Ghobril and M. W. Grinstaff, *Chem. Soc. Rev.*, 2015, **44**, 1820–1835.
- N. Annabi, A. Fathi, S. M. Mithieux, P. Martens, A. S. Weiss and F. Dehghani, *Biomaterials*, 2010, **32**, 1517–1525.
- S. Yan, T. Wang, L. Feng, J. Zhu, K. Zhang, X. Chen, L. Cui and J. Yin, *Biomacromolecules*, 2014, **15**, 4495–4508.
- J. Yang, M. A. C. Stuart and M. Kamperman, *Chem. Soc. Rev.*, 2014, **43**, 8271–8298.
- Y. Mu and X. Wan, *Macromol. Rapid Commun.*, 2016, **37**, 545–550.
- I. V. Yannas, E. Lee, D. P. Orgill, E. M. Skrabut and G. F. Murphy, *Proc. Natl. Acad. Sci. U. S. A.*, 1989, **86**, 933–937.
- J. Zeltinger, J. K. Sherwood, D. A. Graham, R. Mueller and L. G. Griffith, *Tissue Eng.*, 2001, **7**, 557–572.

- 49 Q. L. Loh and C. Choong, *Tissue Eng., Part B*, 2013, **19**, 485–502.
- 50 S.-M. Lien, L.-Y. Ko and T.-J. Huang, *Acta Biomater.*, 2009, **5**, 670–679.
- 51 Y. Chiu, M. Cheng, H. Engel, S. Kao, J. C. Larson, S. Gupta and E. M. Brey, *Biomaterials*, 2011, **32**, 6045–6051.
- 52 K. Kim, M. Shi, M.-Y. Koh, J. H. Ryu, M. S. Lee, S. Hong and H. Lee, *Adv. Healthcare Mater.*, 2015, **25**, 2402–2410.
- 53 H. Lee, J. Rho and P. B. Messersmith, *Adv. Mater.*, 2009, **21**, 431–434.
- 54 S. H. Ku, J. Ryu, S. K. Hong, H. Lee and C. B. Park, *Biomaterials*, 2010, **31**, 2535–2541.